Inorganic Chemistry

Article

pubs.acs.org/IC

Preparation and Structure of Uranium-Incorporated $Gd_2Zr_2O_7$ Compounds and Their Thermodynamic Stabilities under Oxidizing and Reducing Conditions

Mohsin Jafar, Suhas B. Phapale, Balaji P. Mandal, Ratikant Mishra, and Avesh K. Tyagi*

Chemistry Division, Bhabha Atomic Research Centre, Mumbai 400085, India

Supporting Information

ABSTRACT: $Gd_2Zr_2O_7$ is being contemplated as a futuristic matrix for the incorporation of high-level radioactive nuclear waste. This compound has the unique ability to incorporate several fission products and heavy metal ions like uranium and thorium into its lattice sites without undergoing structural changes. X-ray diffraction analyses of $Gd_{2-x}U_xZr_2O_{7+\delta}$ samples indicate that the parent compound can incorporate a substantial amount of uranium, both under oxidizing and reducing conditions. The oxidation state of these samples was investigated by X-ray photoelectron spectroscopy. The thermodynamic stability of uranium-substituted $Gd_2Zr_2O_7$ is an important parameter that will govern the long-term storage of uranium and minor actinides in this matrix. High-temperature calorimetry has been used to investigate the stability of the $Gd_{2-x}U_xZr_2O_{7+\delta}$ $(0.00 \le x \le 0.15)$ compositions. The standard molar free energy of the formation of $Gd_{2-x}U_xZr_2O_{7+\delta}$ $(0.00 \le x \le 0.15)$ compositions has been estimated. From the free energy of formation data, the sample corresponding to $x = 0.15$ was found to be most stable in the $Gd_{2-x}U_xZr_2O_{7+\delta}$ $(0.00 \le x \le 0.15)$ series. The relative stabilities of U^{4+} and U^{6+} substituted gadolinium zirconate have been discussed on the basis of the charge on the uranium ion and the incorporation of corresponding extra oxygen atoms into the lattice for charge compensation.

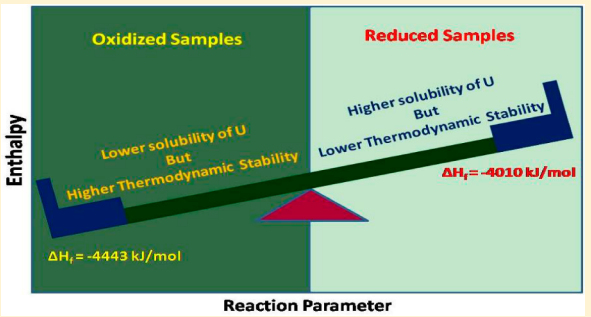

INTRODUCTION

A borosilicate glass matrix has been widely used as a host matrix for the immobilization of high-level nuclear waste (HLW).[1] However, glasses are metastable, which might be a concern. Moreover, under accidental conditions, water ingression into the glass matrixes can cause the formation of water-soluble salts, which may increase the leachability of some of the constituents.[2] Therefore, the stress has been laid on designing new types of matrixes such as glass ceramics, ceramics, etc., for the immobilization of nuclear HLW.[3−5] Ceramic matrixes have several advantages such as high thermodynamic stability, lower leachability, and high chemical and radiation stabilities, which are important parameters for the immobilization of actinides for long-term purposes.[6−11]

Among the ceramics, pyrochlores, hollandite, zirconolite, etc., have been considered as suitable host matrixes for the disposal of radioactive waste because of their excellent stability even in nonstoichiometric compositions, which makes them amenable for aliovalent ion substitution.[12−14] The pyrochlore family of the compounds has the general formula $A_2B_2O_7$, where A is the larger cation and B is the smaller cation, with the radius ratio (r_A/r_B) within 1.46−1.6. Cation A is most commonly a trivalent rare-earth ion but can also be a divalent or monovalent ion, whereas cation B can be a 3d, 4d, or 5d element in its suitable oxidation state.[15,16] The nonstoichiometric phase formation is expected to arise with substitution at either the A or B site or both sites by aliovalent cations.[17−19] The fixation of rare-earth elements, which are considered as surrogates for minor actinides in the pyrochlore matrix, was successfully demonstrated earlier.[5,20−22]

Among the pyrochlores, $Gd_2Zr_2O_7$ is a versatile matrix that has the unique ability to incorporate a large amount of fission products and heavy metals like thorium, etc., expected to be generated from advanced nuclear fuels.[5,6] $Gd_2Zr_2O_7$, which is at the borderline of pyrochlore and defect fluorite with a low r_A/r_B radius ratio, is an extremely radiation-resistant matrix that can withstand both high- and low-energy radiation environments. It has been reported that, under high irradiation condition, $Gd_2Zr_2O_7$ does not amorphize but transforms to the fluorite form.[10,16−23]

The immobilization of uranium in a very stable and durable matrix is a viable option for a safer environment. In addition, UO_2 is a good surrogate for NpO_2 and, hence, can be used to simulate data on the NpO_2 incorporation in pyrochlores.[24] Recently, a few groups have reported the incorporation of uranium in the $Gd_2Zr_2O_7$ matrix.[21,25,26] Surprisingly, the literature does not render any information on how the incorporation of heavy elements like thorium and uranium affects the thermodynamic stability of $Gd_2Zr_2O_7$ as a host matrix. It is, therefore, important to investigate the thermodynamic stability of the parent $Gd_2Zr_2O_7$ matrix and the effect of

Received: June 10, 2015
Published: September 17, 2015

DOI: 10.1021/acs.inorgchem.5b01300
Inorg. Chem. 2015, 54, 9447−9457

the incorporation of uranium and/or other radionuclides on its thermodynamic stability. In this study, careful structural refinements were performed to determine the upper solubility limits of uranium, in both hexavalent and tetravalent oxidation states, in the fluorite form of $Gd_2Zr_2O_7$. The standard molar enthalpies of formation ($\Delta_f H_{298}^\circ$) of $Gd_{2-x}U_xZr_2O_{7+\delta}$ were determined by employing a high-temperature calorimetric technique. The standard molar free energy of formation of these compositions has been estimated.

EXPERIMENTAL SECTION

Preparation and Characterization. A series of compositions with the general chemical formula $Gd_{2-x}U_xZr_2O_{7+\delta}$ ($0.0 \le x \le 0.25$) were prepared by a gel-combustion method. Gd_2O_3 (Indian Rare Earths Ltd., purity 99.9%) and U_3O_8 was kept overnight at 1073 K for preheating. Gd_2O_3 was dissolved in a minimum volume of concentrated HNO_3 until a colorless and transparent solution was obtained. The stoichiometric amount of $ZrO(NO_3)_2$ (Loba Chemie, 44% metal basis) and U_3O_8 powder were added to this solution. The resulting solution was boiled until a transparent yellow solution was obtained. Finally, glycine was added to the boiling solution in a fuel-deficient ratio, and the solution was further heated until a viscous gel was obtained. The temperature of the hot plate was then raised ~673 K for autoignition, resulting in the formation of yellowish-orange fine powders.

The products were then calcined at 873 K for 1 h to remove any carbonaceous impurities. Part of the powders was further heated at 1373 K for 8 h in a 92% argon−8% hydrogen flowing atmosphere. Another part of the products was heated at 1373 K for 8 h in static air. All of the samples were characterized by powder X-ray diffraction (XRD) technique. High-temperature XRD studies were also performed on these samples in the range of 298−1273 K in static air. The powder XRD patterns were recorded on a PANalytical X-Pert powder X-ray diffractometer using Cu Kα (λ = 1.5406 and 1.5444 Å) radiation. Structural analyses of the samples were performed using the Rietveld refinement program *Fullprof-2000*.[27] The microstructures of the samples were examined by using scanning electron microscopy (SEM; model AIS 210, Mirero Inc., Seongnam-si, South Korea). X-ray photoelectron spectroscopy (XPS) studies were performed using a SPECS XPS instrument with a PHOBIOS 100/150 delay line detector with 385 W, 13.85 kV, and 175.6 nA (sample current). An Al Kα (1486.6 eV) dual anode was used as the source. The C 1s peak (284.5 eV) was used as an internal reference for the absolute binding energy.

High-Temperature Calorimetry. The standard molar enthalpies of formation of $Gd_{2-x}U_xZr_2O_{7+\delta}$ (x = 0.0,0.05, 0.1, 0.15) were determined by measuring the enthalpy of dissolution of $Gd_{2-x}U_xZr_2O_{7+\delta}$ compounds and their constituent oxides such as Gd_2O_3(s), U_3O_8(s), and ZrO_2(s) in a liquid Na_2O + MoO_3 solvent (3:4 molar ratio) at 986 K, employing a high-temperature Calvet calorimeter (Setaram model HT-1000). The calorimeter has an isothermal alumina block that contains two identical one-end-closed alumina cells surrounded by a series of thermopiles. The temperature of the isothermal block was measured using a Pt−Pt 10% rhodium thermocouple (±0.1 K). Further details of the experimental measurements have been described elsewhere.[28] The heat calibration was carried out using a synthetic sapphire sample (NIST SRM-720).

The compounds and their component oxides were found to be completely soluble in the calorimetric solvent, i.e., Na_2O + MoO_3 (3:4 molar mixture) at 986 K. This solvent was prepared by heating a mixture of perfectly dried Na_2CO_3 (BDH, reagent grade) and MoO_3 (BDH, reagent grade) in the appropriate molar ratio in a platinum disk at 973 K. Na_2CO_3 decomposes to Na_2O, forming a eutectic mixture with MoO_3. The melt was maintained at 973 K for 6 h for further homogenization. The mass loss of the solvent was monitored to ensure the correct stoichiometry of the melt, which was compensated by mixing the required amount of MoO_3, followed by remelting. The entire substance was removed from the platinum disk by slowly scratching the melt and ground again to obtain a uniform powder. The solvent powder was characterized by chemical analysis and XRD techniques. The atom percents of molybdenum, sodium, and oxygen obtained from chemical analysis of the solvent were found to be 16.2 ± 0.2, 23.4 ± 0.3, and 60.4 ± 0.4, respectively. No other chemical impurity could be detected. Na_2O + MoO_3 powder prepared in the same batch was used in all of the reaction enthalpy measurements, so as to ensure reproducibility of the thermodynamic data.

About 6 g of the Na_2O + MoO_3 (3:4 molar) solvent was taken in each of the two identical platinum tubes, which act as a protective lining and having an outer diameter matching exactly with the alumina reaction cell for proper thermal contact. The reaction cell assembly was slowly lowered into the calorimeter, which was programmed up to 986 K at a heating rate of 0.5 K/min and maintained at 986 ± 0.05 K during the whole experiment.

The reaction tubes were equilibrated inside the chamber for 12 h until a steady baseline for the heat flux signal was achieved. The slope of the baseline of the differential heat flow signal was nearly zero because the heat effect due to any small loss of the volatile components will get nullified because the same effect was present in the sample and reference cells. Small pellets containing a few milligrams of the component oxides and $Gd_{2-x}U_xZr_2O_{7+\delta}$ products were dropped from room temperature to the reaction cell containing liquid solvent maintained at 986 K, and the corresponding enthalpy change was determined by integrating the heat flow signal with respect to time. The time required for completion of the reaction was determined by recording the heat flow signal (J/g) for different time intervals. Completion of the dissolution reaction was concluded when a steady baseline was observed and the values of the reaction enthalpy obtained as a function of time converged into a constant value. For each dissolution experiment, the reaction time was determined and the heat flow signals were recorded for the same time period for all experiments. Similarly, for each experiment, fresh solvent was used so that the similar dilution condition was maintained. The amounts of component oxides and products dropped into solvent were chosen in such a manner that the concentrations of gadolinium, uranium, and zirconium in the solvent remained well below 1 atom %. The infinite dilution condition was carefully established by repeating the dissolution experiments on the same batch of the solvent. The consistency in the values of the reaction per unit mass of the reactants is indicative of the fact that the infinite dilution condition was maintained during the measurements. After each measurement, the sample was slowly withdrawn from the calorimeter chamber and allowed to cool to room temperature. The frozen liquid was characterized by EDS analysis to determine the uniform distribution of the solute in the solvent and to ascertain the infinite dilution condition of the solute in the solvent. Oxygen bubbling experiments into the solvent were deliberately avoided because it was very difficult to get a steady baseline under oxygen bubbling conditions. In addition, the solvent particles borne by the oxygen flow often react while the structural material (quartz), producing undesirable heat effects, and may affect the reproducibility of the results. Hence, the calorimetric experiments were performed in static air.

RESULTS AND DISCUSSION

XRD. The gel-combustion synthesis method is widely used to prepare nanocrystalline oxide materials.[29] It is a redox reaction between an oxidant (metal nitrate) and a fuel (like glycine, citric acid, etc.). The oxidizing valency of $UO_2(NO_3)_2$, $Gd(NO_3)_3$, and $ZrO(NO_3)_2$ are −10, −15, and −10, respectively, while the reducing valency of glycine is +9, calculated by considering the valencies of individual ions. The exothermic properties of the combustion reaction depend on the fuel content and can be varied by altering the oxidant-to-fuel ratio. In the present case, a fuel-deficient ratio (1:0.6) was selected. The product obtained in each of the combustion reactions was calcined at 873 K for 1 h to remove all of the carbonaceous residues.

DOI: 10.1021/acs.inorgchem.5b01300
Inorg. Chem. 2015, 54, 9447−9457

The formation of the phases in the system $Gd_{2-x}U_xZr_2O_{7+\delta}$ ($0.0 \le x \le 0.25$) was inferred by characterizing the as-prepared samples by a powder XRD technique. XRD patterns of the calcined products showed broad peaks due to the nanocrystalline nature of the samples (Figure 1). All of the patterns

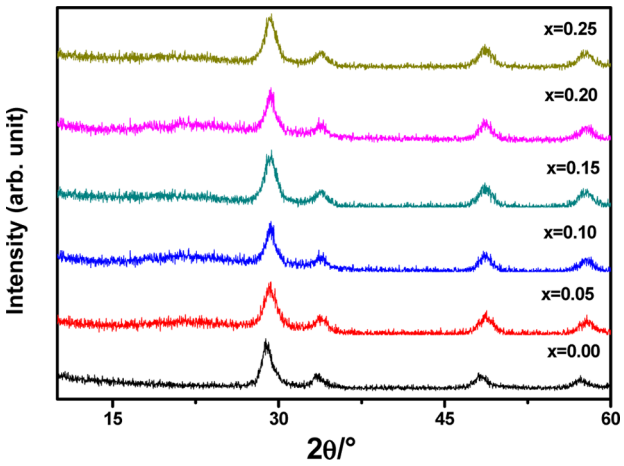

Figure 1. XRD patterns of $Gd_{2-x}U_xZr_2O_{7+\delta}$ ($0.0 \le x \le 0.25$) samples calcined at 873 K for 1 h.

showed a resemblance with that of the fluorite structure of $Gd_2Zr_2O_7$. Moreover, the XRD patterns did not show any peaks corresponding to Gd_2O_3, UO_x, and ZrO_2. The general composition of the products obtained after calcination can be represented as $Gd_{2-x}U_xZr_2O_{7+\delta}$. However, because of the broadness of the peaks of the as-prepared samples, further characterization of the phases present and meaningful elucidation of the structural parameters were not done.

Subsequently, the samples were reduced in the presence of an Ar/H_2 (92:8) atmosphere at 1373 K for 8 h. XRD patterns of all of the reduced samples in the system $Gd_{2-x}U_xZr_2O_{7+\delta}$ ($0.0 \le x \le 0.25$) confirm the formation of a monophasic fluorite-type structure, as shown in Figure 2a. In spite of pyrochlore being the most favorable structure for $Gd_2Zr_2O_7$, the absence of superstructure peaks at $2\theta \sim 14.5°$, 28.1°, and 37.2° (using Cu Kα as the radiation source) in its XRD pattern indicates that the sample, prepared and heat-treated under these conditions, crystallizes in the fluorite structure. In the case of pyrochlores having a r_A/r_B ratio at the border of pyrochlore and fluorite lattices, the reaction conditions and post heat treatment may lead to the formation of either pyrochlore- or fluorite-type structures.[5] The most plausible explanation for crystallization of $Gd_2Zr_2O_7$ in the fluorite phase in the present study could be the lack of ordering of the cations in the $Gd_2Zr_2O_7$ structure because the maximum temperature used for its preparation in this study was 1373 K. It is known that in order to get $Gd_2Zr_2O_7$ in the pyrochlore form, it needs to anneal at temperatures of about 1473−1573 K, followed by slow cooling.[5] Structural analysis has been done using the Rietveld refinement program *Fullprof-2000*. Initially, the background parameters and scale factor were adjusted. The background was fitted with a sixth-order polynomial. The diffraction peak profile was fitted with a pseudo-Voigt profile function, and then *U*, *V*, and *W* were refined. No absorption parameter and displacement were considered during the refinement. The refined parameters are summarized in Table 1, and representative Rietveld refinement plots are shown in Figure 2b. Because of the inherent structural disorder in the

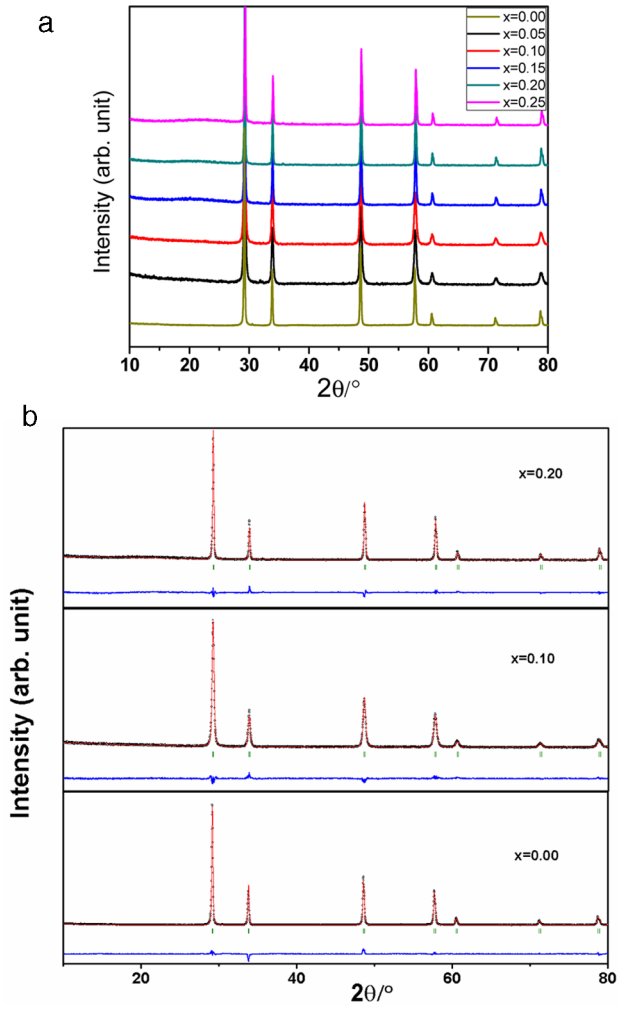

Figure 2. (a) XRD patterns of $Gd_{2-x}U_xZr_2O_{7+\delta}$ ($0.0 \le x \le 0.25$) samples annealed in Ar/H_2 (92:8) at 1373 K for 8 h. All of the compositions crystallize in the fluorite structure. (b) Representative Rietveld refinement plots for the nominal compositions in the series $Gd_{2-x}U_xZr_2O_{7+\delta}$ ($0.0 \le x \le 0.25$) heated in a reducing atmosphere.

present Gd−U−Zr−O system, the quality of the fitting of the (200) peak is slightly poor because this plane in the defect-fluorite structure is constituted by cations only.

It is observed that, with an increase in the concentration of U^{4+}, a steady decrease in the lattice parameters of the compositions was observed. There are two antagonistic factors affecting the variation in the lattice parameter as a function of the uranium content in this system. First, the lower ionic radius of U^{4+} (1.00 Å in 8-fold coordination) compared to that of Gd^{3+} (1.05 Å) could lead to a decrease in the overall lattice parameter.[30] At the same time, substitution of U^{4+} in place of Gd^{3+} may also lead to unit cell dilation because of an extra half-oxygen, which gets incorporated into the system for charge balance accompanied by the incorporation of each U^{4+} ion. The observed net decrease in the lattice parameter suggests that the effect of the smaller ionic radius of U^{4+} compared to that of Gd^{3+} is predominant over the incorporated extra oxygen in the lattice.

In order to investigate the solubility of uranium in the hexavalent oxidation state, all of the samples were annealed in static air at 1373 K for 8 h and characterized by powder XRD. The absence of additional peaks in the XRD patterns for the

DOI: 10.1021/acs.inorgchem.5b01300
Inorg. Chem. 2015, 54, 9447−9457

Table 1. Rietveld Refined Parameters of $Gd_{2-x}U_xZr_2O_{7+\delta}$ ($0.0 \le x \le 0.25$) Compositions after Annealing at Ar/H_2 (92:8) at 1373 K for 8 h

sample	$Gd_2Zr_2O_7$	$Gd_{1.95}U_{0.05}Zr_2O_{7+\delta}$	$Gd_{1.90}U_{0.10}Zr_2O_{7+\delta}$	$Gd_{1.85}U_{0.15}Zr_2O_{7+\delta}$	$Gd_{1.80}U_{0.20}Zr_2O_{7+\delta}$	$Gd_{1.75}U_{0.25}Zr_2O_{7+\delta}$
a (Å)	5.2621(1)	5.2601(1)	5.2591(1)	5.2578(4)	5.2569(1)	5.2559(3)
U	0.277(3)	0.931(1)	0.499(1)	0.077(3)	0.074(3)	0.086(4)
V	−0.234(2)	−0.462(1)	−0.183(9)	−0.014(7)	−0.051(3)	−0.068(2)
W	0.073(5)	0.148(2)	0.099(2)	0.031(2)	0.033(5)	0.038(1)
χ^2	1.01	1.45	1.71	1.63	1.94	2.40
R_p	8.36	9.01	9.67	9.56	8.29	11.5
R_{wp}	11.72	12.2	12.8	12.8	10.8	14.5
R_{exp}	11.71	10.11	9.76	10.02	7.75	9.34
space group	$Fm\bar{3}m$	$Fm\bar{3}m$	$Fm\bar{3}m$	$Fm\bar{3}m$	$Fm\bar{3}m$	$Fm\bar{3}m$

compositions x = 0.0−0.15 in $Gd_{2-x}U_xZr_2O_{7+\delta}$ indicates that the samples up to x = 0.15 crystallize in a single phase under the oxidizing conditions. However, the compositions with x = 0.20 and 0.25 show impurity peaks, suggesting the commencement of phase separation leading to a biphasic nature of the products. The comparatively poor solubility of uranium into the fluorite structure of $Gd_2Zr_2O_7$ under this condition could be due to the oxidation of U^{4+} to U^{6+} at this temperature. The oxidation of U^{4+} to U^{6+} leads to the incorporation of a large number of extra oxygen atoms into the $Gd_2Zr_2O_7$ lattice. Plausibly, at and after this particular composition (x = 0.2), the lattice could not accommodate the large amount of excess oxygen, which results in segregation of the secondary phase (Figure 3).

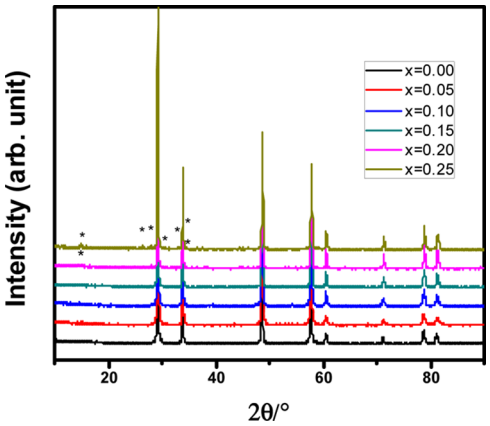

Figure 3. XRD patterns of $Gd_{2-x}U_xZr_2O_{7+\delta}$ ($0.0 \le x \le 0.25$) after heat treatment in air at 1373 K for 8 h. Asterisks indicate the unidentified secondary phase.

The lattice parameter of the oxidizing samples decreases with an increase in the uranium content due to the much smaller ionic radius of U^{6+} compared to that of Gd^{3+} in the $Gd_{2-x}U_xZr_2O_{7+\delta}$ system. Because the ionic radius of U^{6+} is smaller than that of U^{4+}, the decrease in the lattice parameter is more prominent in oxidized samples compared to that of the samples prepared under reducing conditions (Figure 4). The lattice parameter does not vary for the samples x = 0.20 and 0.25, which further confirms their biphasic nature. The amount of the secondary phase is so small that it could not be identified.

In situ high-temperature XRD studies on the reduced samples were carried out until 1273 K in static air to investigate the stability of the U^{4+} substituted $Gd_2Zr_2O_7$ samples under an oxidizing environment. It was observed that all of the samples

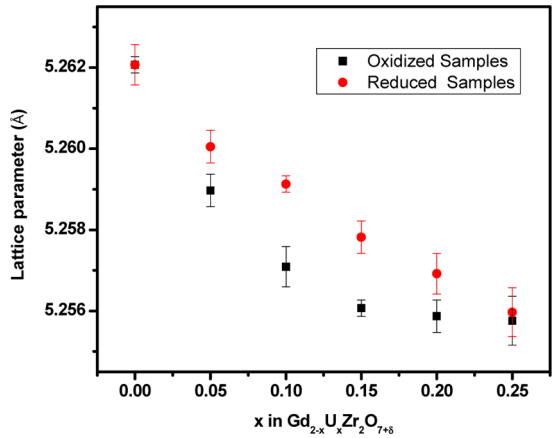

Figure 4. Variation of the lattice parameter upon substitution of uranium at the gadolinium site in $Gd_{2-x}U_xZr_2O_{7+\delta}$ (reduced and oxidized samples).

remain monophasic with the exception of $Gd_{1.75}U_{0.25}Zr_2O_{7+\delta}$, where a segregated secondary phase consisting of $UZrO_x$ was observed at 1173 K onward. The typical XRD patterns of $Gd_{1.95}U_{0.05}Zr_2O_{7+\delta}$ and $Gd_{1.75}U_{0.25}Zr_2O_{7+\delta}$, respectively, at different temperatures are shown in Figure 5a,b. The systematic shift of peaks toward lower diffraction angle with an increase in the temperature suggests the expansion of the lattice (Figure 5a). The intensity of the peaks in Figure 5b of the secondary phases ($UZrO_x$) in the XRD patterns of $Gd_{1.75}U_{0.25}Zr_2O_{7+\delta}$ at 1173 and 1273 K and room temperature was too small to refine; therefore, the exact phase identification could not be done. All of the samples showed a steady increase in the cell parameter with an increase in the temperature (Figure 6). When the reduced samples are heated in air, two phenomena occur simultaneously, viz., oxidation of uranium in the substituted samples and thermal expansion of the unit cell. In this situation, there are three main controlling factors for variation of the unit cell with temperature: (a) thermal expansion of the unit cell parameters with an increase in the temperature, (b) expansion of the lattice parameters due to the incorporation of additional oxygen in the lattice as a consequence of the oxidation of U^{4+} to U^{6+} and (c) shrinkage of the lattice parameter due to a decrease in the ionic radii of uranium by the aerial oxidation of U^{4+} to U^{6+} at higher temperature. It is observed that thermal expansion of the unit cell parameter of pure $Gd_2Zr_2O_7$ is more than that of the uranium-substituted samples (Figure 6). Moreover, in all uranium-substituted samples, the unit cell parameter after cooling to room temperature is found to be lower than the cell parameter recorded initially at room temperature. This further

DOI: 10.1021/acs.inorgchem.5b01300
Inorg. Chem. 2015, 54, 9447−9457

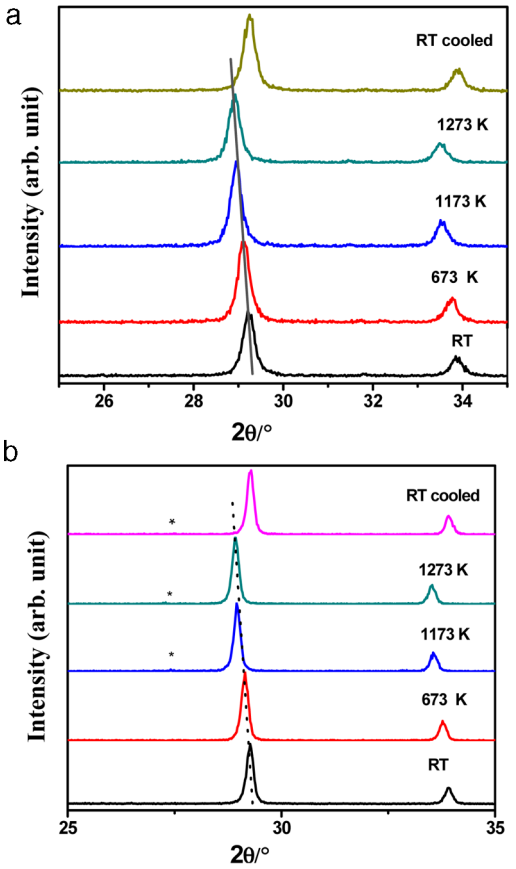

Figure 5. High-temperature XRD patterns of (a) $Gd_{1.95}U_{0.05}Zr_2O_{7+\delta}$ and (b) $Gd_{1.75}U_{0.25}Zr_2O_{7+\delta}$. A solid line has been used to show the shift in the peak position with variation in the temperature. The asterisk indicates the presence of a secondary phase.

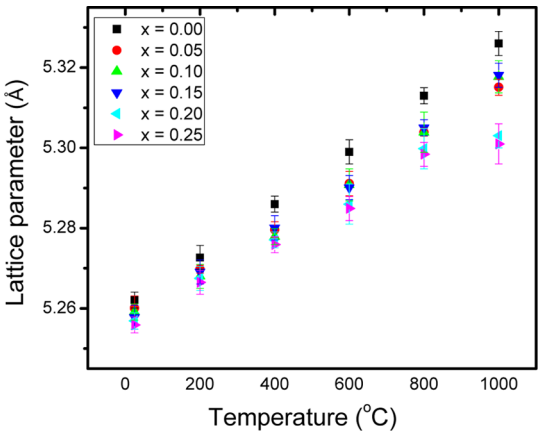

Figure 6. Variation of the lattice parameter of the sample $Gd_{2-x}U_xZr_2O_{7+\delta}$ ($0.00 \leq x \leq 0.25$) with temperature.

indicates that the oxidation of uranium under a static air environment causes a decrease in its ionic radius, leading to shrinkage in the lattice parameter. Additionally, the extra oxygen incorporated in the lattice during oxidation did not result in phase segregation up to $x = 0.15$. The above phenomena also reveal that shrinkage of the lattice parameters due to the aerial oxidation of uranium is much more dominant than expansion of the lattice due to the incorporation of oxygen into the lattice. An ideal fluorite lattice can accommodate eight oxygen atoms. In addition, the samples prepared in this study were anion-deficient fluorites, which will further support the accommodation of excess oxygen due to the oxidation of U^{4+} to U^{6+}. Hence, the oxidation of uranium within the lattice did not result in structural rearrangement of the fluorite structure of the samples until $x = 0.15$. In the composition $Gd_{1.75}U_{0.25}Zr_2O_{7+\delta}$, as soon as the secondary phase appeared above 1173 K, the rate of increase of the cell parameters was reduced.

XPS. The determination of the oxidation state of uranium in samples prepared under different experimental conditions (oxidized and reduced) is required for ascertaining inferences drawn by XRD. The XPS spectra of two representative oxidized and reduced samples corresponding to $x = 0.15$ in $Gd_{2-x}U_xZr_2O_{7+\delta}$ have been given in Figure 7. The position of

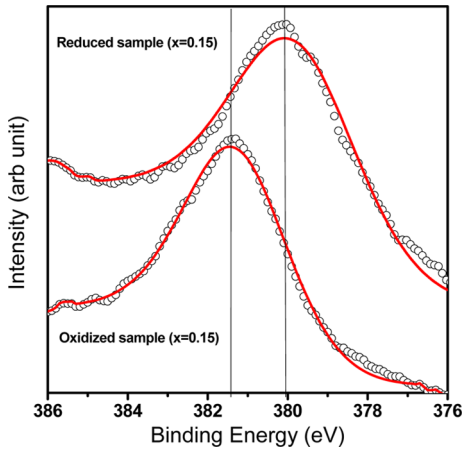

Figure 7. XPS spectra of uranium ($4f_{7/2}$) of reduced and oxidized samples having the nominal composition $Gd_{1.85}U_{0.15}Zr_2O_{7+\delta}$.

the $4f_{7/2}$ peak in the XPS spectrum is directly related to the uranium oxidation state. It was reported earlier that the $4f_{7/2}$ peak of U^{6+} appears at 381.0−381.5 eV.[31,32] In our oxidized sample ($x = 0.15$), the $4f_{7/2}$ peak appears at 381.35 eV. This indicates that the uranium in this composition is in the 6+ oxidation state. On the other hand, the $4f_{7/2}$ peak appears at 380.05 eV in the reduced sample corresponding to $x = 0.15$ in $Gd_{2-x}U_xZr_2O_{7+\delta}$. Bera et al. and Boily et al. reported that the $4f_{7/2}$ peak of U^{4+} appears in the range of 379.8−380.15 eV.[32,33] The observed XPS data confirm that uranium in the reduced sample is in the +4 oxidation state. Boily et al. have reported that the $4f_{7/2}$ peak of U^{5+} appears at 380.4 eV. Because in these compositions no XPS peak appears at 380.4 eV, it can be inferred that the samples were free from any impurity that contains uranium in the +5 oxidation state. XPS spectra of reduced and oxidized uranium-substituted $Gd_2Zr_2O_7$ ($x = 0.10$) have been given as Supporting Information (Figure S1).

SEM Studies. In order to further confirm the phase information on the compositions, secondary electron (SE) and backscattered electron (BSE) imaging have been performed on all of the samples. The SEM micrographs of the reduced sample ($x = 0.25$) reveal it to be monophasic in nature (Figure 8a,b), which is in agreement with the XRD results. It can be seen from the micrographs that the samples under investigation are porous in nature. The reason could be that the samples have been sintered at relatively lower temperature.

The BSE images of the oxidized samples of $x = 0.15$, 0.2, and 0.25 are shown in parts a, c, and e of Figure 9, respectively. The micrograph at Figure 9a (for the sample $x = 0.15$) clearly indicates the monophasic nature of the composition. These

DOI: 10.1021/acs.inorgchem.5b01300
Inorg. Chem. 2015, 54, 9447−9457

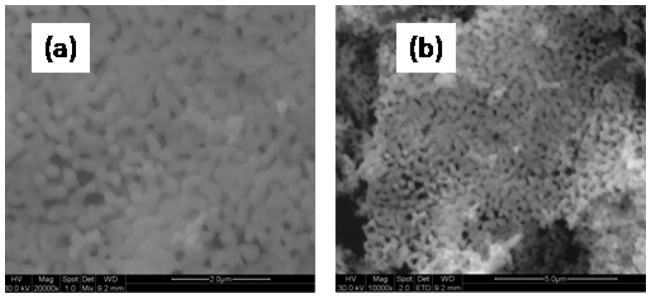

Figure 8. SEM images of $Gd_{2-x}U_xZr_2O_{7+\delta}$ samples: (a) BSE and (b) SE images of the x = 0.25 reduced sample.

SEM micrographs of the biphasic samples were recorded by focusing the electron beam on the secondary-phase-rich zones. Therefore, the other two BSE images (Figure 9c,e), which correspond to the samples x = 0.20 and 0.25, show the presence of the secondary phase. Another important observation is the increase in the quantity of the impurity phase from x = 0.20 to 0.25. The SE images for the samples x = 0.15, 0.2, and 0.25 are shown in parts b, d, and f of Figure 9, respectively. Features similar to those described in the case of BSE images have been found in these images also.

Standard Molar Enthalpy of Formation of $Gd_{2-x}U_xZr_2O_{7+\delta}$ ($0.0 \le x \le 0.15$). Standard molar enthalpies of formation of monophasic compounds of $Gd_{2-x}U_xZr_2O_{7+\delta}$ ($0.0 \le x \le 0.15$) prepared in both oxidizing and reducing conditions were derived from the values of the enthalpy of dissolution of $Gd_{2-x}U_xZr_2O_{7+\delta}$ ($0.0 \le x \le 0.15$) samples and their component oxides such as Gd_2O_3(s), U_3O_8(s), and ZrO_2(s) in a liquid Na_2O + MoO_3 (3:4 molar ratio) solvent maintained at 986 K.[34−36]

The representative heat flow signals for dissolution of $Gd_{2-x}U_xZr_2O_{7+\delta}$ ($0.0 \le x \le 0.15$) oxidized and reduced compounds normalized to 10 mg each in liquid Na_2O + MoO_3

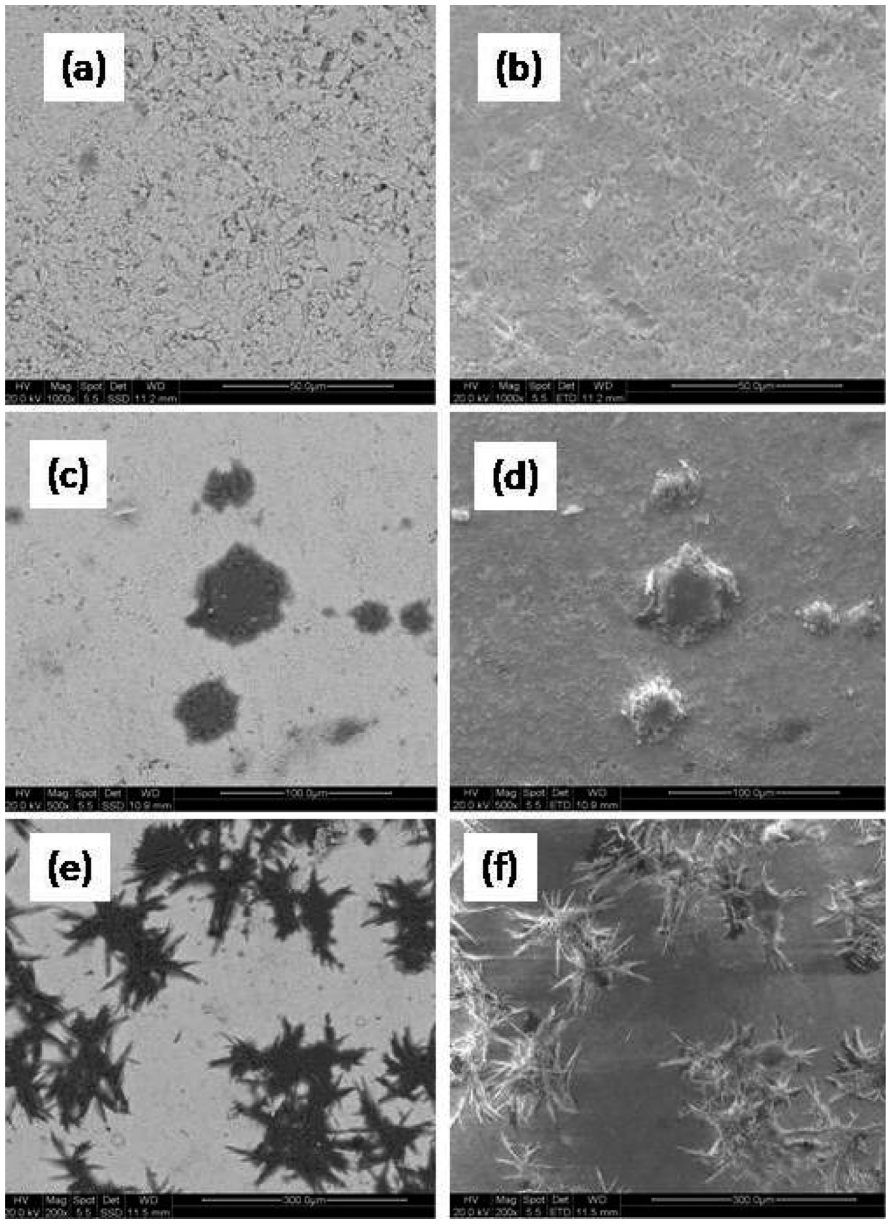

Figure 9. BSE images of (a) x = 0.15, (c) x = 0.20, and (e) x = 0.25 and SE images of (b) x = 0.15, (d) x = 0.20, and (f) x = 0.25.

DOI: 10.1021/acs.inorgchem.5b01300
Inorg. Chem. 2015, 54, 9447−9457

(3:4 molar ratio) dropped from room temperature to liquid-solvent 986 K are shown in Figure 10a,b. In each dropping, an

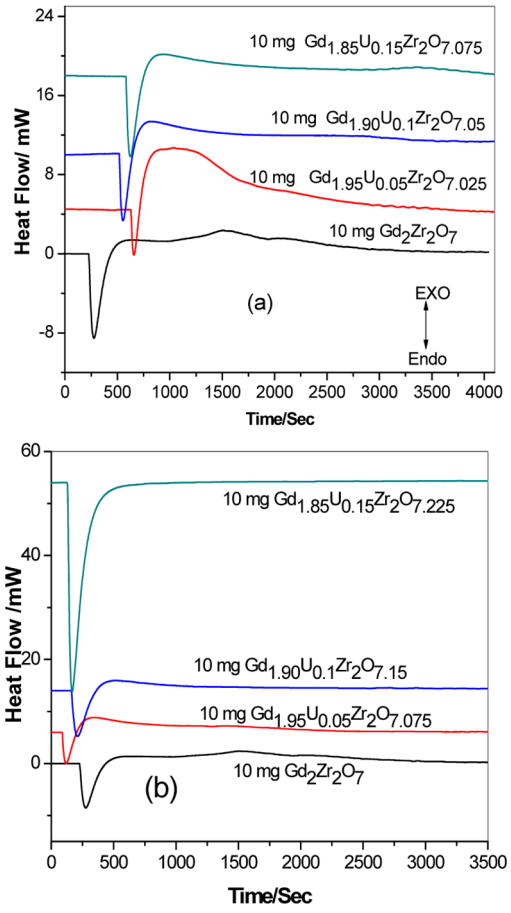

Figure 10. Heat flow signals for dissolution of $Gd_{2-x}U_xZr_2O_{7+\delta}$ ($0.0 \leq x \leq 0.15$) (a) reduced and (b) oxidized compounds (normalized to 10 mg each) in liquid $Na_2O + MoO_3$ (3:4 molar ratio) dropped from room temperature to liquid-solvent 986 K.

endothermic signal was observed. The completion of the reaction between the reactants and solvent was monitored by recording the heat flow signal for different time intervals. A steady baseline in the heat flow signal was observed after 3500 s of sample dropping, beyond which no significant change in the heat flow values was observed. Therefore, a total of 1 h of measurement time was selected for each experiment. The overall heat effect for dissolution in a liquid $Na_2O + MoO_3$ (3:4 molar ratio) solvent was calculated considering both endothermic and exothermic effects using the *SETSOFT* software supplied along with the instrument. The values of the molar enthalpies of dissolution of $Gd_{2-x}U_xZr_2O_{7+\delta}$ ($0.0 \leq x \leq 0.15$) and their component oxides such as Gd_2O_3(s), UO_2(s), and ZrO_2(s) in a liquid $Na_2O + MoO_3$ (3:4 molar ratio) solvent maintained at 986 K are given in Table 2. This enthalpy change was attributed to the sum of the endothermic heat effects due to the enthalpy increment from 298 to 986 K and the heat effect due to the chemical reaction of the solute with the solvent at 986 K.

The frozen products from each calorimetric measurement dissolved in distilled water at ~330 K gave clear solutions, indicating that the added reactants are completely dissolved in the solvent and dispersed as ions, not as compounds. The SEM images for the Na_2O and MoO_3 (3:4 molar mixture) frozen products containing less than 1 atom % of $Gd_{2-x}U_xZr_2O_{7+\delta}$ (until $x = 0.15$), obtained after the reaction, indicate that gadolinium, zirconium, and uranium ions are uniformly distributed in the whole solvent matrix (Supporting Information, Figure S2). When reduced $Gd_{2-x}U_xZr_2O_{7+\delta}$ is dropped in the solvent, the possibility of MoO_3 reduction to MoO_2 by U^{4+} is not ruled out. In order to ascertain the final oxidation state of molybdenum in the solidified melt recovered after the calorimetric experiment, XPS studies were performed. The $3d_{5/2}$ peak of molybdenum was found to be at 233.2 eV. As per the NIST database, it should be at 233.15 eV.[37] These studies revealed that the final oxidation state of molybdenum in the solidified melt is +6 (Supporting Information, Figure S3). A plausible explanation could be that the resulting MoO_2 (if formed) is oxidized to MoO_3 by gaining oxygen from the air. Because the amount of oxygen in equilibrium with the solvent is plentiful compared to the very small quantity of U^{4+}, it is expected that, during a prolonged measurement time of 1 h, the reduced Mo^{4+} sample will regain oxygen from the static air, considering fast diffusion of ions at 986 K in the liquid medium (Supporting Information). The uranium in reduced $Gd_{2-x}U_xZr_2O_{7+\delta}$ after the calorimetric experiment was also found to be in the +6 oxidation state (Supporting Information, Figure S4). Thus, the oxidation state of uranium, in samples prepared under reduced and oxidized conditions, after drop calorimetric experiments is +6.

The standard molar enthalpies of formation of $Gd_{2-x}U_xZr_2O_{7+\delta}$ ($0.0 \leq x \leq 0.15$) compounds were derived using the thermochemical cycles given in Table 3. The values for molar enthalpies of dissolution ($\Delta H_{dissolution}$) of $Gd_{2-x}U_xZr_2O_{7+\delta}$ ($0.0 \leq x \leq 0.15$) and their component oxides such as Gd_2O_3(s), U_3O_8(s), and ZrO_2(s) were combined, together with other auxiliary data such as the standard molar enthalpies of formation of Gd_2O_3(s), ZrO_2(s), and U_3O_8(s) from the literature,[34−36,38,39] to derive the standard molar enthalpy of formation for $Gd_{2-x}U_xZr_2O_{7+\delta}$ ($0.0 \leq x \leq 0.15$) at 298 K prepared under reducing and oxidizing conditions. The values are listed in Table 3.

It is observed here that the enthalpy of formation of $Gd_2Zr_2O_7$ obtained from the present study differs from the reported value for the compound by Helean et al. by ~70 kJ/mol.[35] This difference of ~1.74% may arise because of the difference in the nature of the sample. In the reported data, the sample was prepared at 1873 K, at which the sample adopts a pyrochlore structure.[35] On the other hand, samples in the present work were prepared at 1373 K, leading to formation of the fluorite structure. A heat treatment at higher temperature (1873 K for 50 h[35]) is expected to result in a sample with slightly higher thermodynamic stability due to better annealing, leading to a relatively defect-free material. In addition, there could be some difference in the literature values of the constituents used in the thermochemical cycle in the derivation of the standard molar enthalpy of formation, which contributes to the slight difference in value.

From the experimentally obtained enthalpy of formation data, it could be observed that the stability of the $Gd_{2-x}U_xZr_2O_{7+\delta}$ compounds prepared under reducing conditions decreases by 84.9 kJ/mol by the addition of 2.5 atom % U^{4+} at Gd^{3+} site ($x = 0.05$). Upon further addition of U^{4+} ions, the stability of the compound improves, as shown in Figure 11. The marginal decrease in the stability of the composition corresponding to $x = 0.05$ (reduced) in $Gd_{2-x}U_xZr_2O_{7+\delta}$ could be plausibly explained by two combined effects, i.e., an increase

DOI: 10.1021/acs.inorgchem.5b01300
Inorg. Chem. 2015, 54, 9447−9457

Table 2. Heat of Dissolution of $Gd_{2-x}U_xZr_2O_{7+\delta}$ (Oxidized/Reduced) And Their Component Oxides[a]

compound	mass (m and mg)	ΔH (J/g)	ΔH_T (kJ/mol)
$Gd_2Zr_2O_7$(s); mol wt = 608.948	26.5	−271.63	−165.41
	25.2	−266.20	−162.10
	24.7	−271.34	−165.23
	20.1	−268.42	−163.45
			ave: −164.05 ± 1.57
$Gd_{1.95}U_{0.05}Zr_2O_{7.025}$(s) (reduced); mol wt = 613.387	35.6	−418.01	−256.40
	22.4	−416.23	−255.31
	13.0	−415.95	−255.14
	21.5	−417.48	−256.08
			ave: −255.73 ± 0.60
$Gd_{1.90}U_{0.10}Zr_2O_{7.05}$(s) (reduced); mol wt = 617.826	27.9	−300.01	−185.35
	31.6	−298.65	−184.51
	29.4	−301.02	−185.98
	31.5	−298.03	−184.13
			ave: −184.99 ± 0.83
$Gd_{1.85}U_{0.15}Zr_2O_{7.075}$(s) (reduced); mol wt = 622.265	10.3	−283.31	−176.29
	12.5	−287.41	−178.85
	14.5	−284.86	−177.26
	21.3	−285.91	−177.91
			ave: −177.59 ± 1.08
$Gd_{1.95}U_{0.05}Zr_2O_{7.075}$(s) (oxidized); mol wt = 614.187	11.0	−263.10	−161.60
	9.7	−259.90	−159.63
	20.0	−261.52	−160.62
	12.0	−257.84	−158.36
			ave.: −160.05 ± 1.38
$Gd_{1.90}U_{0.10}Zr_2O_{7.15}$(s) (oxidized); mol wt = 619.43	22.5	−164.61	−101.96
	22.8	−165.11	−102.27
	13.1	−164.10	−101.65
	17.6	−162.52	−100.67
			ave: −101.64 ± 0.69
$Gd_{1.85}U_{0.15}Zr_2O_{7.225}$(s) (oxidized); mol wt = 624.665	5.4	413.81	258.49
	5.0	407.15	254.33
	5.3	405.53	253.32
	4.5	409.07	255.53
			ave: 255.42 ± 2.24
ZrO_2(s); mol wt = 123.224	11.7	356.60	43.94
	13.2	357.91	44.10
	9.3	355.83	43.85
	17.1	354.79	43.72
			ave: 43.90 ± 0.16
U_3O_8; mol wt = 842.09	31.6	87.80	73.94
	26.6	88.13	74.21
	25.2	87.14	73.38
	13.9	88.78	74.76
			ave: 74.07 ± 0.57
Gd_2O_3; mol wt = 362.50	23.4	−656.30	−237.91
	21.3	−657.12	−238.21
	19.7	−655.03	−237.45
	16.4	−654.74	−237.34
			ave: −237.73 ± 0.41

[a]A solvent consisting of Na_2O + MoO_3 (3:4) was used. The experiment was done in static air condition with no oxygen bubbling. The molar enthalpies of dissolution of $Gd_2Zr_2O_7$(s), $Gd_{1.95}U_{0.05}Zr_2O_{7.025}$(s), $Gd_{1.90}U_{0.10}Zr_2O_{7.05}$(s), $Gd_{1.85}U_{0.15}Zr_2O_{7.175}$(s) (reduced), $Gd_{1.95}U_{0.05}Zr_2O_{7.075}$(s), $Gd_{1.90}U_{0.10}Zr_2O_{7.15}$(s), $Gd_{1.85}U_{0.15}Zr_2O_{7.175}$(s) (oxidized), ZrO_2(s), U_3O_8(s), and Gd_2O_3(s) in 6 g of Na_2O + MoO_3 3:4 molar ratio at T = 986 K; m denotes the mass of the sample dissolved; ΔH is the measured energy change per unit mass, and ΔH_T is the molar enthalpy of the solution.

in the repulsive force due to excess oxide ions (destabilizing factor) and also an increase in the attractive force due to the higher positive charge of the doped U^{4+} in place of Gd^{3+} ion (stabilizing factor). The destabilizing factor appears to be the major contributor for the composition corresponding to x = 0.05, but with increasing U^{4+} content (i.e., for composition x = 0.10 and 0.15), an increase in the positive attractive force (stabilizing factor) became more dominant, thereby increasing the stability of the compositions with increasing incorporation of U^{4+}. However, in the case of the $Gd_{2-x}U_xZr_2O_{7+\delta}$ compounds prepared by annealing at 1373 K in air (under oxidizing condition), the enthalpy of formation is found to increase progressively with an increase in the U^{6+} content up to x = 0.15. The increase in the formation enthalpy with an increase in the U^{6+} content could be explained by the higher columbic attractive force between U^{6+} and O^{2-} ions, which overrides the repulsive force of excess oxide ion (destabilizing factor) and stabilizes the compound. In addition, the presence of a U^{6+} ion leads to a decrease in the unit cell parameter, which results in an increase in the lattice packing density, which might be another plausible reason for the higher stability of U^{6+}-substituted $Gd_2Zr_2O_7$ samples. In addition, the incorporation of uranium might increase the disorder in the lattice, which also could enhance the thermodynamic stability. It may be noted that all of the thermodynamic experiments were repeated eight times, and the observed trend remained the same. Thus, the observed trend in the thermodynamic stability of $Gd_2Zr_2O_7$ as a function of U^{4+} and U^{6+} incorporation is highly reproducible and is an intrinsic behavior. A detailed theoretical work is required to calculate the lattice energy as a function of these two competing factors. The exact theoretical delineation of these two factors will enable us to understand the observed trend of the thermodynamic stability as a function of x in this series. However, it is important to summarize here that once U^{4+} is incorporated in the $Gd_2Zr_2O_7$ lattice, the stability of the matrix increases. The stability of the x = 0.15 sample (oxidized) is 440.16 kJ/mol higher than that of parent $Gd_2Zr_2O_7$, which is a remarkable observation from an application point of view. The matrix becomes very stable if uranium gets oxidized in the lattice, which is a significant result from the point of view of long-term storage.

Estimation of the Standard Molar Free Energy of Formation of $Gd_{2-x}U_xZr_2O_{7+\delta}$ ($0.0 \le x \le 0.15$). In order to find the influence of the entropy on the stability of $Gd_{2-x}U_xZr_2O_{7+\delta}$ ($0.0 \le x \le 0.15$) compounds, their Gibbs free energy of formation at 298 K of this series was estimated. The standard molar Gibbs energy of formation at 298 K of $Gd_{2-x}U_xZr_2O_{7+\delta}$ (x = 0, 0.05, 0.10, and 0.15) was derived using the measured standard molar enthalpy of formation data of $Gd_{2-x}U_xZr_2O_{7+\delta}$ (x = 0, 0.05, 0.10, and 0.15) together with their respective estimated standard molar entropy change ($\Delta_fS_{298}^\circ$) for the formation reaction using the relation

$$\Delta_fG_{298}^\circ = \Delta_fH_{298}^\circ - T\Delta_fS_{298}^\circ \quad (1)$$

DOI: 10.1021/acs.inorgchem.5b01300
Inorg. Chem. 2015, 54, 9447−9457

Table 3. Thermochemical Cycles for Enthalpy of Formation of $Gd_{2-x}U_xZr_2O_{7+\delta}$ (Oxidized/Reduced)[a]

reaction	ΔH_i	$\Delta H_{dissolution}$ (kJ/mol^{-1})
$Gd_2Zr_2O_7(s, 298K) + (sln) = Gd_2O_3(sln) + 2ZrO_2(sln)$	ΔH_1	−164.04 ± 1.57
Reduced		
$Gd_{1.95}U_{0.05}Zr_2O_{7.025}(s, 298K) + (sln) + 0.0167O_2(g) = 0.975Gd_2O_3(sln) + 0.0167U_3O_8(sln) + 2ZrO_2(sln)$	$\Delta H_{1a(red)}$	−255.73 ± 0.60
$Gd_{1.90}U_{0.10}Zr_2O_{7.05}(s, 298K) + (sln) + 0.0333O_2(g) = 0.95Gd_2O_3(sln) + 0.0333U_3O_8(sln) + 2ZrO_2(sln)$	$\Delta H_{1b(red)}$	−184.99 ± 0.83
$Gd_{1.85}U_{0.15}Zr_2O_{7.075}(s, 298K) + (sln) + 0.050O_2(g) = 0.925Gd_2O_3(sln) + 0.050U_3O_8(sln) + 2ZrO_2(sln)$	$\Delta H_{1c(red)}$	177.59 ± 1.08
Oxidized		
$Gd_{1.95}U_{0.05}Zr_2O_{7.075}(s, 298K) + (sln) = 0.975Gd_2O_3(sln) + 0.0166U_3O_8(sln) + 2ZrO_2(sln)$	$\Delta H_{1a(oxi)}$	−160.05 ± 1.38
$Gd_{1.90}U_{0.10}Zr_2O_{7.15}(s, 298K) + (sln) = 0.975Gd_2O_3(sln) + 0.0333U_3O_8(sln) + 2ZrO_2(sln)$	$\Delta H_{1b(oxi)}$	−101.64 ± 0.69
$Gd_{1.85}U_{0.15}Zr_2O_{7.225}(s, 298K) + (sln) = 0.975Gd_2O_3(sln) + 0.050U_3O_8(sln) + 2ZrO_2(sln)$	$\Delta H_{1c(oxi)}$	255.42 ± 2.24
$ZrO_2(s, 298K) + (sln) = ZrO_2(sln)$	ΔH_2	43.90 ± 0.16
$U_3O_8(s, 298K) + (sln) = U_3O_8(sln)$	ΔH_3	74.07 ± 0.57
$Gd_2O_3(s, 298K) + (sln) = Gd_2O_3(s)$	ΔH_4	−237.73 ± 0.41
$2Gd(s, 298K) + \frac{3}{2}O_2(g) = Gd_2O_3(s)$	ΔH_5	−1815.86 ± 16.74
$3U(s, 298K) + 4O_2(g) = U_3O_8(s)$	ΔH_6	−3573.55 ± 3.68
$Zr(s, 298K) + O_2(g) = ZrO_2(s)$	ΔH_7	−1100.81 ± 2.09
$2Gd(s, 298K) + 2Zr(s, 298K) + 3.5O_2(g) = Gd_2Zr_2O_7(s, 298K)$	$\Delta_fH_{298}^\circ$	−4003.37 ± 17.08
Reduced		
$1.95Gd(s, 298K) + 0.05U(s, 298K) + 2Zr(s, 298K) + 3.5125O_2(g) = Gd_{1.95}U_{0.05}Zr_2O_{7.025}(s, 298K)$	$\Delta_fH_{298,Reduced}^\circ$	−3918.78 ± 16.60
$1.90Gd(s, 298K) + 0.10U(s, 298K) + 2Zr(s, 298K) + 3.525O_2(g) = Gd_{1.9}U_{0.1}Zr_2O_{7.05}(s, 298K)$		−3996.27 ± 16.20
$1.85Gd(s, 298K) + 0.15U(s, 298K) + 2Zr(s, 298K) + 3.588O_2(g) = Gd_{1.85}U_{0.15}Zr_2O_{7.175}(s, 298K)$		−4010.77 ± 15.81
Oxidized		
$1.95Gd(s, 298K) + 0.05U(s, 298K) + 2Zr(s, 298K) + 3.5124O_2(g) = Gd_{1.95}U_{0.05}Zr_2O_{7.075}(s, 298K)$	$\Delta_fH_{298,Oxidized}^\circ$	−4014.11 ± 16.65
$1.90Gd(s, 298K) + 0.01U(s, 298K) + 2Zr(s, 298K) + 3.575O_2(g) = Gd_{1.9}U_{0.1}Zr_2O_{7.15}(s, 298K)$		−4079.62 ± 16.20
$1.85Gd(s, 298K) + 0.15U(s, 298K) + 2Zr(s, 298K) + 3.663O_2(g) = Gd_{1.85}U_{0.15}Zr_2O_{7.325}(s, 298K)$		−4443.78 ± 15.93

[a]Reaction scheme for the standard molar enthalpy of formation of $Gd_{2-x}U_xZr_2O_{7+\delta}(s)$(Red/Oxi), where M(sln) = dilute solution of species M in 6 g of a 3:4 liquid Na_2O/MoO_3 molar solvent maintained at 986 K.

$$\Delta_fH_{298}^\circ(Gd_2Zr_2O_7) = -\Delta H_1 + 2\Delta H_2 + \Delta H_4 + \Delta H_5 + 2\Delta H_7$$

$$\Delta_fH_{298}^\circ(Gd_{1.95}U_{0.05}Zr_2O_{7+\delta})(Red/Oxi) = -\Delta H_{1a(red/oxi)} + 2\Delta H_2 + 0.0166\Delta H_3 + 0.975\Delta H_4 + 0.975\Delta H_5 + 0.0166\Delta H_6 + 2\Delta H_7$$

DOI: 10.1021/acs.inorgchem.5b01300
Inorg. Chem. 2015, 54, 9447−9457

Table 3. continued

$$\Delta_f H_{298}^{\circ}(Gd_{1.90}U_{0.10}Zr_2O_{7+\delta})(Red/Oxi) = -\Delta H_{1b(red/oxi)} + 2\Delta H_2 + 0.0333\Delta H_3 + 0.95\Delta H_4 + 0.95\Delta H_5 + 0.0333\Delta H_6 + 2\Delta H_7$$

$$\Delta_f H^{\circ}_{298}(Gd_{1.85}U_{0.15}Zr_2O_{7+\delta})(Red/Oxi) = -\Delta H_{1c(red/oxi)} + 2\Delta H_2 + 0.05\Delta H_3 + 0.925\Delta H_4 + 0.925\Delta H_5 + 0.05\Delta H_6 + 2\Delta H_7$$

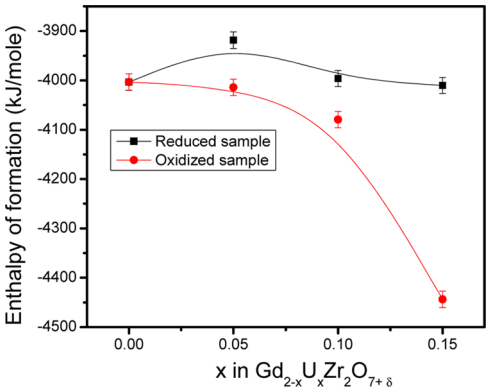

Figure 11. Enthalpy of formation of $Gd_{2-x}U_xZr_2O_{7+\delta}$ (both oxidized and reduced samples).

The entropy change for the above formation reaction can be expressed as

$$\Delta_f S_{298}^{\circ}(Gd_{2-x}U_xZr_2O_{7+\delta}) = S^{\circ}(Gd_{2-x}U_xZr_2O_{7+\delta}) - [(2-x)S^{\circ}(Gd, s) + xS^{\circ}(U, s) + 2S^{\circ}(Zr, s) + (7+\delta)/2S^{\circ}(O_2, g)] \quad (2)$$

The standard molar entropy of $Gd_{2-x}U_xZr_2O_{7+\delta}$ (x = 0, 0.05, 0.10, and 0.15) oxidized and reduced samples were estimated by adding the entropy values of the constituent oxides in their respective molar proportion using Neumann Kopp rule and the entropy of the constituent elements have been taken from the literature.[40] The estimated standard molar entropy of formation $\Delta_f S^0_{298}$ of $Gd_{2-x}U_xZr_2O_{7+\delta}$ (x = 0, 0.05, 0.10 and 0.15are given in Table 4. It may be noted that in the calculation of entropy for the $Gd_{2-x}U_xZr_2O_{7+\delta}$ disordered systems, the contribution of the configurational entropy has not been considered here. The standard molar free energy of formation $\Delta_f G^o_{298}$ of $Gd_{2-x}U_xZr_2O_{7+\delta}$ (x = 0, 0.05, 0.10 and 0.15) at 298 K calculated using the experimental values of standard molar enthalpy of formation ($\Delta_f H^o_{298}$) and the estimated standard molar entropy of formation ($\Delta_f S^0_{298}$) are listed in Table 4.

From Table 4, it can be observed that the estimated entropy of formation for the $Gd_{2-x}U_xZr_2O_{7+\delta}$ (x = 0, 0.05, 0.10, and 0.15) series changed marginally as a function of the composition, which have been reflected in the estimated values of the standard molar free energy of formation of the compounds. This result corroborates the stability patterns of the series derived from the enthalpy of formation data.

CONCLUSIONS

A series of compositions with the general formula $Gd_{2-x}U_xZr_2O_{7+\delta}$ ($0.0 \le x \le 0.25$) have been prepared by the gel combustion method followed by heat treatment under oxidizing and reducing conditions at 1373 K for 8 h. A considerable amount of uranium (x = 0.25) could be incorporated in the $Gd_2Zr_2O_7$ lattice in a reducing environment even at relatively lower temperature. The compositions with lower uranium loading (until x = 0.15) remain stable even under an oxidizing environment until the studied temperature, i.e., 1273 K; however, high uranium-containing compositions (x= 0.25) show phase separation under these conditions. The oxidation state of these samples was investigated by XPS. The thermodynamic stabilities of uranium-substituted gadolinium zirconates $Gd_{2-x}U_xZr_2O_{7+\delta}$ ($0.0 \le x \le 0.15$) were determined. The trend in the thermodynamic stability in the Gd−U−Zr−O system, under oxidizing and reducing conditions, was explained by two competing effects, namely, the incorporation of extra-interstitial oxygen ions, which lowers the stability, and an enhanced electrostatic force of attraction between U^{4+}/U^{6+} and O^{2-} ions, which increases the stability. The enthalpy of formation suggests that the incorporation of U^{4+} at the gadolinium site marginally increases the stability of uranium-incorporated $Gd_2Zr_2O_7$ (x > 0.10), whereas U^{6+} stabilizes the matrix significantly in the entire studied composition range. These results will help to design newer matrixes for long-term storage of nuclear waste in ceramic host matrixes.

Table 4. Thermodynamic Parameters for $Gd_{2-x}U_xZr_2O_{7+\delta}$ (x = 0, 0.05, 0.10, and 0.15) Compositions

condition	sample	$\Delta_f H_{298}^{\circ}$ (kJ/mol) (measured)	$\Delta_f S_{298}^{\circ}$ (J/mol·K) (estimated)	$\Delta_f G_{298}^{\circ}$ (kJ/mol) (estimated)
pristine	$Gd_2Zr_2O_7$	−4003.37 ± 17.11	253.08	−4078.8
reduced	$Gd_{1.95}U_{0.05}Zr_2O_{7.025}$	−3918.43 ± 16.81	253.12	−3993.9
	$Gd_{1.9}U_{0.10}Zr_2O_{7.05}$	−3996.27 ± 16.62	253.17	−4071.7
	$Gd_{1.85}U_{0.15}Zr_2O_{7.075}$	−4010.77 ± 16.43	253.21	−4086.3
oxidized	$Gd_{1.95}U_{0.05}Zr_2O_{7.075}$	−4014.05 ± 16.86	253.99	−4089.8
	$Gd_{1.9}U_{0.10}Zr_2O_{7.15}$	−4079.62 ± 16.62	254.87	−4155.6
	$Gd_{1.85}U_{0.15}Zr_2O_{7.225}$	−4443.53 ± 16.55	255.79	−4519.8

DOI: 10.1021/acs.inorgchem.5b01300
Inorg. Chem. 2015, 54, 9447−9457

■ ASSOCIATED CONTENT

Supporting Information

The Supporting Information is available free of charge on the ACS Publications website at DOI: 10.1021/acs.inorgchem.5b01300.

Figures S1−S4 (PDF)

■ AUTHOR INFORMATION

Corresponding Author

*E-mail: aktyagi@barc.gov.in. Phone: 0091-22-2559 5330. Fax: 0091-22-25505151.

Notes

The authors declare no competing financial interest.

■ ACKNOWLEDGMENTS

The authors thank Dr. S. N. Achary for useful discussion . The authors thank S. Kaity, D. Sahoo, and Dr. K. Bhattacharyya, BARC, for their contribution in the recording of SEM images, sample preparation, and XPS studies and discussion. The authors are also grateful to Dr V. K. Jain, Head, Chemistry Division, BARC, for his interest in this work.

■ REFERENCES

(1) Kleykamp, H. *J. Nucl. Mater.* **1999**, *275*, 1−11.
(2) Ojovan, M. I.; Lee, W. E. *An Introduction to Nuclear Waste Immobilization*; Elsevier Ltd.: Oxford, U.K., 2005; pp 213−267.
(3) McCarthy, G. J.; White, W. B.; Roy, R.; Scheetz, B. E.; Komarneni, S.; Smith, D. S.; Roy, D. M. *Nature* **1978**, *273*, 216−217.
(4) Ringwood, A. E.; Kesson, S. E.; Ware, N. G.; Hibberson, W.; Major, A. *Nature* **1979**, *278*, 219−223.
(5) Mandal, B. P.; Pandey, M.; Tyagi, A. K. *J. Nucl. Mater.* **2010**, *406*, 238−243.
(6) Vance, E. R. *MRS Online Proc. Libr.* **2006**, *985*, 135−140.
(7) Ewing, R. C. *Proc. Natl. Acad. Sci. U. S. A.* **1999**, *96*, 3432−3439.
(8) Vance, E. R.; Lumpkin, G. R.; Carter, M. L.; Cassidy, D. J.; Ball, C. J.; Day, R. A.; Begg, B. D. *J. Am. Ceram. Soc.* **2002**, *85*, 1853−1859.
(9) Mcglinn, P. J.; Advocat, T.; Leturcq, G.; Mcleod, T. I.; Aly, Z.; Yee, P. *MRS Online Proc. Libr.* **2006**, *932*, 575−581.
(10) Sickafus, K. E.; Minervini, L.; Grimes, R. W.; Valdez, J. A.; Ishimaru, M.; Li, F. *Science* **2000**, *289*, 748−751.
(11) Zhang, J.; Lian, J.; Zhang, F.; Wang, J.; Fuentes, A. F.; Ewing, R. C. *J. Phys. Chem. C* **2010**, *114* (27), 11810−11815.
(12) Jafar, M.; Sengupta, P.; Achary, S. N.; Tyagi, A. K. *J. Am. Ceram. Soc.* **2014**, *97*, 609−616.
(13) Achary, S. N.; Sali, S. K.; Kulkarni, N. K.; Krishna, P. S. R.; Shinde, A. B.; Tyagi, A. K. *Chem. Mater.* **2009**, *21*, 5848−5859.
(14) Babu, G. S.; Valant, M.; Page, K.; Llobet, A.; Kolodiazhnyi, T.; Axelsson, A. K. *Chem. Mater.* **2011**, *23* (10), 2619−2625.
(15) Subramanian, M. A.; Aravamudan, G.; Subba Rao, G. V. *Prog. Solid State Chem.* **1983**, *15*, 55−143.
(16) Mandal, B. P.; Tyagi, A. K. *J. Alloys Compd.* **2007**, *437*, 260−263.
(17) Zinkevich, M.; Wang, Ch.; Morales, F. M.; Rühle, M.; Aldinger, F. *J. Alloys Compd.* **2005**, *398*, 261−268.
(18) Zhang, Z.; Middleburgh, S. C.; de los Reyes, M.; Lumpkin, G. R.; Kennedy, B. J.; Blanchard, P. E. R.; Reynolds, E.; Jang, L. Y. *J. Phys. Chem. C* **2013**, *117*, 26740−26749.
(19) Reynolds, E.; Blanchard, P. E. R.; Kennedy, B. J.; Ling, C. D.; Liu, S. *Inorg. Chem.* **2013**, *52*, 8409−8415.
(20) Patwe, S. J.; Tyagi, A. K. *Ceram. Int.* **2006**, *32*, 545−548.
(21) Govindan Kutty, K. V.; Asuvathraman, R.; Raja Madhavan, R.; Jena, H. *J. Phys. Chem. Solids* **2005**, *66*, 596−601.
(22) Mandal, B. P.; Shukla, R.; Achary, S. N.; Tyagi, A. K. *Inorg. Chem.* **2010**, *49*, 10415−10421.
(23) Patel, M. K.; Vijayakumar, V.; Avasthi, D. K.; Kailas, S.; Pivin, J. C.; Grover, V.; Mandal, B. P.; Tyagi, A. K. *Nucl. Instrum. Methods Phys. Res., Sect. B* **2008**, *266*, 2898−2901.
(24) Forbes, T. Z.; Burns, P. C.; Skanthakumar, S.; Soderholm, L. *J. Am. Chem. Soc.* **2007**, *129* (10), 2760−2761.
(25) Gregg, D. J.; Zhang, Y.; Zhang, Z.; Karatchevtseva, I.; Blackford, M. G.; Triani, G.; Lumpkin, G. R.; Vance, E. R. *J. Nucl. Mater.* **2013**, *438*, 144−153.
(26) Zhang, F. X.; Lang, M.; Tracy, C.; Ewing, R. C.; Gregg, D. J.; Lumpkin, G. R. *J. Solid State Chem.* **2014**, *219*, 49−54.
(27) Carjaval R. J. *Fullprof2k, Multi pattern Rietveld refinement program*, version 1.6; July 2000.
(28) Phapale, S.; Das, D.; Mishra, R. *J. Chem. Thermodyn.* **2013**, *63*, 74−77.
(29) Purohit, R. D.; Sharma, B. P.; Pillai, K. T.; Tyagi, A. K. *Mater. Res. Bull.* **2001**, *36*, 2711−2721.
(30) Shannon, R. D. *Acta Crystallogr., Sect. A: Cryst. Phys., Diffr., Theor. Gen. Crystallogr.* **1976**, *32*, 751−767.
(31) Goldik, J. S.; Nesbitt, H. W.; Noel, J. J.; Shoesmith, D. W. *Electrochim. Acta* **2004**, *49*, 1699−1709.
(32) Bera, S.; Sali, S. K.; Sampath, S.; Narasimhan, S. V.; Venugopal, V. *J. Nucl. Mater.* **1998**, *255*, 26−33.
(33) Boily, J. − F.; Ilton, E. S. *Surf. Sci.* **2008**, *602*, 3637−3646.
(34) Lee, T. A.; Navrotsky, A.; Molodetsky, I. *J. Mater. Res.* **2003**, *18*, 908−918.
(35) Helean, K. B.; Begg, B. D.; Navrotsky, A.; Ebbinghaus, B.; Weber, W. J.; Ewing, R. C. *MRS Online Proc. Libr.* **2000**, *663*, 691−697.
(36) Guo, X.; Ushakov, S. V.; Labs, S.; Curtius, H.; Bosbach, D.; Navrotsky, A. *Proc. Natl. Acad. Sci. U. S. A.* **2014**, *111* (50), 17737−17742.
(37) Nefedov, V. I.; Gati, D.; Dzhurinskii, B. F.; Sergushin, N. P.; Salyn, Y. V. *Zh. Neorg. Khim.* **1975**, *20*, 2307.
(38) Kubaschewski, O.; Alcock, C. B.; Spencer, P. J. *Materials Thermochemistry*, 6th ed.; Pergamon Press: Oxford, U.K., 1993.
(39) Guo, X.; Szenknect, S.; Mesbah, A.; Labs, S.; Clavier, N.; Poinssot, C.; Ushakov, S. V.; Curtius, H.; Bosbach, D.; Ewing, R. C.; Burns, P. C.; Dacheux, N.; Navrotsky, A. *Proc. Natl. Acad. Sci. U. S. A.* **2015**, *112*, 6551−6555.
(40) Belov G. V.; Trusor B. G. *ASTD-Computer aided Reference Book in Thermodynamical, Thermochemical and Thermophysical Properties of Species*, version 2 (C); Moscow, 1983−1995.

DOI: 10.1021/acs.inorgchem.5b01300
Inorg. Chem. 2015, 54, 9447−9457